A Review of Modeling Approaches for Predicting Frost Growth and Defrosting on Tube-Fin Heat Exchangers

Preprint

Zechao Lu, Ransisi Huang, and Jason Woods

National Renewable Energy Laboratory

Presented at the 20th International Refrigeration and Air Conditioning Conference
West Lafayette, Indiana
July 15-18, 2024

NREL is a national laboratory of the U.S. Department of Energy
Office of Energy Efficiency & Renewable Energy
Operated by the Alliance for Sustainable Energy, LLC

This report is available at no cost from the National Renewable Energy Laboratory (NREL) at www.nrel.gov/publications.

Contract No. DE-AC36-08GO28308

Conference Paper
NREL/CP-5500-89649
September 2024

A Review of Modeling Approaches for Predicting Frost Growth and Defrosting on Tube-Fin Heat Exchangers

Preprint

Zechao Lu, Ransisi Huang, and Jason Woods

National Renewable Energy Laboratory

Suggested Citation
Lu, Zechao, Ransisi Huang, and Jason Woods. 2024. *A Review of Modeling Approaches for Predicting Frost Growth and Defrosting on Tube-Fin Heat Exchangers: Preprint*. Golden, CO: National Renewable Energy Laboratory. NREL/CP-5500-89649. https://www.nrel.gov/docs/fy24osti/89649.pdf.

NREL is a national laboratory of the U.S. Department of Energy
Office of Energy Efficiency & Renewable Energy
Operated by the Alliance for Sustainable Energy, LLC

This report is available at no cost from the National Renewable Energy Laboratory (NREL) at www.nrel.gov/publications.

Contract No. DE-AC36-08GO28308

Conference Paper
NREL/CP-5500-89649
September 2024

National Renewable Energy Laboratory
15013 Denver West Parkway
Golden, CO 80401
303-275-3000 • www.nrel.gov

NOTICE

This work was authored by the National Renewable Energy Laboratory, operated by Alliance for Sustainable Energy, LLC, for the U.S. Department of Energy (DOE) under Contract No. DE-AC36-08GO28308. Funding provided the U.S. Department of Energy Office of Energy Efficiency and Renewable Energy Building Technologies Office. The views expressed herein do not necessarily represent the views of the DOE or the U.S. Government. The U.S. Government retains and the publisher, by accepting the article for publication, acknowledges that the U.S. Government retains a nonexclusive, paid-up, irrevocable, worldwide license to publish or reproduce the published form of this work, or allow others to do so, for U.S. Government purposes.

This report is available at no cost from the National Renewable Energy Laboratory (NREL) at www.nrel.gov/publications.

U.S. Department of Energy (DOE) reports produced after 1991 and a growing number of pre-1991 documents are available free via www.OSTI.gov.

Cover Photos by Dennis Schroeder: (clockwise, left to right) NREL 51934, NREL 45897, NREL 42160, NREL 45891, NREL 48097, NREL 46526.

NREL prints on paper that contains recycled content.

A Review of Modeling Approaches for Predicting Frost Growth and Defrosting on Tube-Fin Heat Exchangers

Zechao LU[1], Ransisi HUANG[1], Jason WOODS[1]*

[1]National Renewable Energy Laboratory, Building Technology Science Center

Golden, Colorado, United States

* Corresponding Author: Jason.Woods@nrel.gov

ABSTRACT

Frost formation and growth on the evaporator surface is a common process that deteriorates the air-refrigerant heat transfer and restricts airflow. This degrades the performance of the vapor compression system by increasing temperature lift and air-side pressure drop. To accurately predict these effects during coil frosting, as well as the energy use and duration of the defrost process, there is a need to estimate the heat and mass transfer, momentum transport, and solid-liquid and liquid-vapor phase change. Therefore, in the past few decades, continuous effort has been made to model frosting and defrosting processes using approaches ranging from empirical correlations to computational fluid dynamic models. To provide a clearer overview for researchers, engineers, and manufacturers in this field, this paper provides a comprehensive literature review for frosting and defrosting models. The paper begins with theoretical background of frost formation and defrost processes, and then reviews the common modeling approaches in literature and their underlying assumptions when trying to account for various physical phenomenon. Based on the literature review, the most critical modeling effort for frost formation is the determination of frost densification rate and frost growth rate. Various methods to predict these two parameters are reviewed. Empirical correlations commonly used for frost density and thermal conductivity are presented and compared. For the defrost process, various multi-stage models have been proposed with different assumptions. Some assume the presence of air gap between the tube wall and the frost, while others consider the melted frost flow due to gravity. We also review physics-based and empirical approaches to integrate defrost models into heat pump models. We conclude by identifying research gaps and providing recommendations.

1. INTRODUCTION

Frosting-defrosting cycles cause up to 13% seasonal heating coefficient of performance (COP) degradation for air-source heat pumps (ASHP) (Vocale et al., 2014). When an ASHP operates in heating mode, the outdoor coils work as an evaporator. The heat transfer from the ambient air to the refrigerant causes frost formation when the outdoor coil temperature is below the freezing point during winter operations. As frost accumulates on the coils, the additional thermal resistance and the reduced airflow passage degrades the performance of the heat pump, which requires the heat pump to work in defrost mode to remove the frost on the outdoor coils. The most common defrost method for ASHPs is reverse cycle defrost (RCD), which reverses the refrigerant direction in the heat pump and discharges the hot-gas refrigerant to the outdoor coil. The heat transfer from the refrigerant melts the frost.

Frost formation on heat exchangers can be detrimental to heat exchanger performance. After a continuous layer of frost is formed on the heat exchanger, the frost layer will serve as an extra insulation layer between the heat exchanger surface and the air due to its porous nature. It will increase the thermal resistance of the heat exchanger and reduce the heat transfer rate. In addition, if the frost on the heat exchanger is not removed in a timely manner, the excessive amount of frost can block airflow passage, which will either reduce the airflow rate and decrease the heat transfer rate or increase the fan power. Eventually, the heat exchanger performance degradation leads to a decrease in the heating COP and the heating capacity of the heat pump. Therefore, it is crucial to develop techniques to control frost formation or remove frost (defrost) in a timely and efficient manner from the heat exchanger surface.

Modeling frost formation and defrost processes plays an important role in developing techniques to control and remove frost. Understanding the frost formation process and frost characteristics can help manufacturers design heat exchangers that can slow frost growth and minimize the impact on heat exchanger performance. Frost characteristics are important in designing innovative ways to remove frost, such as ultrasonic vibration (Tan et al., 2019) and shape

morphing fins (Thakkar et al., 2023). For conventional RCD, the ability to predict the defrosting process is a key to developing an energy-efficient defrosting cycle control strategy.

Previous literature reviews focused on frost formation. Iragorry et al. (2004) reviewed properties and models for frost formation. Empirical correlations for frost thermal conductivity, frost average density, and air-frost heat transfer coefficient were collected from the available literature. Comparisons for these correlations were plotted. In addition, mathematical models for frost growth were also collected. However, the models were not categorized in terms of the modeling methods. This study was also limited by publication date. Léoni et al. (2016) conducted a more in-depth review of empirical correlations and mathematical models for frost formation on flat surfaces. Four existing models or correlations for frost thickness on a single horizontal plate were compared with existing experimental results. Five empirical correlations for frost density were compared with experimental results as well. Song and Dang (2018) updated the database from Iragorry et al. (2004) for empirical correlations and mathematical models with newer literature published between 2004 and 2018. A review of measurement techniques for frost density and thickness was also included. Another recent publication reviewed frosting, defrosting, and frost management techniques (Badri et al., 2021). The authors developed a list of experimental studies and theoretical and numerical models for the frost formation process, but without in-depth analysis. This study also contained a review of defrosting techniques, but it did not review the modeling for the defrosting process, and mainly focused on industrial freezer applications. Li and Wang (2021) reviewed mathematical models and computational fluid dynamics (CFD) models that can predict frost formation on a plat plate. The influence of the assumption on absorption rate and supersaturated surface conditions on mathematical models was discussed. However, a review for the defrost process was not included.

Until now, limited reviews existed on a systematic and in-depth summary of empirical correlations and first-principle models for both frosting and defrosting processes. A review of defrosting process models is missing from previous literature. The purpose of this article is not to provide an exhaustive list of previous studies on the models, but to provide an in-depth, systematic, categorized, and easy-to-follow review of models for the frosting and defrosting processes. This review will help researchers, manufacturers, and engineers to obtain an overview of the models, and determine which model is suitable for their applications. Therefore, this paper focuses on empirical correlations and first-principle models that can predict frost characteristics and frost growth, as well as predictive models for multi-stage defrosting processes.

2. FROST MODELING

2.1 Frost Formation Process

Understanding the physical phenomenon of frost formation is the first step in building numerical models for frost formation. In general, frost formation is categorized into three stages, although researchers use different terminologies to describe the three stages. Here, we use the terminology formulated by Tao et al. (1993). Figure 1 shows the process of frost formation on a flat plate under natural convection (Tao et al., 1993). The temperature of the surrounding airflow can be above or below the freezing point. The first stage in the frost formation process is called the dropwise condensation (DWC) period. During this stage, condensing droplets form on the cold flat surface and begin to merge. The droplet diameter increases significantly. With vapor-liquid and liquid-solid phase changes happening at the same time, the droplets merge and solidify. After critical time t_c, these droplets turn into ice particles completely. The critical time t_c is related to ambient conditions, such as temperature, natural/forced convection, etc. After critical time t_c is reached, the solidification and tip-growth period (STG) begins. During this stage, non-uniform frost tips grow on the solid ice droplets. The final stage starts at the transitional time t_t, which is the densification and bulk growth period (DBG). During this stage, the frost is homogeneous for each cross-section perpendicular to the frost growth direction and possesses the characteristics of a porous medium. The structure and characteristics of the frost depend on ambient conditions and the physical and thermodynamic properties of the medium where the frost builds up.

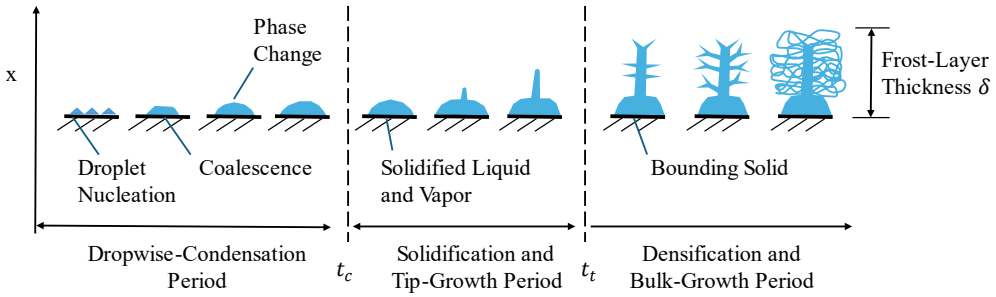

Figure 1: Definition of frost growth periods (Tao et al., 1993)

The physics behind frost formation is complicated and spans multiple scales, especially for DWC and STG. However, these two stages last a very short period compared to DBG. Therefore, engineers usually focus on the third stage (DBG) and rely on macroscopic physical quantities to characterize the frost layer. Quantities such as frost layer thickness and density can be used to quantify the mass of the frost accumulated on the heat exchangers, which can be used to evaluate the impact on the heat exchanger performance. They can be good indicators to determine the intervals for defrost cycle initiation and can be used to optimize defrost control strategies. The frost layer density and thickness also serve as the initial conditions for defrost process modeling. Wrong frost layer properties lead to inaccurate defrost power usage and defrost cycle duration. Therefore, it is important to develop a model that can predict the frost layer thickness and density as a function of time on the heat exchanger surfaces.

For the DBG stage, the frost characteristics include (a) frost layer thickness and growth rate, (b) frost layer density and densification rate, (c) frost thermal conductivity, and frost morphology (porosity and tortuosity), and (d) the air-frost heat and mass transfer coefficient (Song & Dang, 2018). The capabilities to predict these frost characteristics and how they impact the heat exchanger performance are usually of interest for HVAC&R engineers and researchers. Frost growth rates and densification rates dictate the frost accumulation process. Therefore, determination of frost densification and growth rates is essential to modeling frost formation (Qiao et al., 2017). Frost density and thermal conductivity are two important characteristics in determining the frost densification and growth rates (Hermes, 2012; Y. B. Lee & Ro, 2005). Other important frost characteristics on heat exchangers include the air-side pressure drop and fin efficiency degradation.

2.2 Frosting Model on Simple Geometry

The first-principles models for the frost formation process can be divided into two categories, lumped model or 1D model based on the dimension of the model. Early research on frost formation focused on lumped models, where the frost layer is considered a uniform medium. No temperature profile or local water vapor density profile is considered within the frost layer. White and Cremer (1981) developed a lumped model for the frosting process. In the model, the total water vapor mass flow rate from the air stream $\dot{m}_v$ to the frost is divided into two parts. One contributes to frost densification $\dot{m}_\rho$, and the other contributes to frost thickness growth $\dot{m}_\delta$. Through observation from experiments, the authors assumed that the densification mass flow rate is half of the total water vapor mass flow rate. Through energy and mass balance, the frost density and thickness can be predicted. Padhmanabhan et al. (2011) also divided the total mass flow rate $\dot{m}_v$ into $\dot{m}_\rho$ and $\dot{m}_\delta$. The densification mass flow rate $\dot{m}_\rho$ is modeled by assuming the water vapor within the frost layer is saturated. It can be associated with the frost surface temperature using the Clausius-Clapeyron equation. The lumped model created by Fossa and Tanda (2002) did not divide the total mass flow rate into two parts. The frost density and thickness are calculated by correlations and energy and mass balance. It can be concluded that the lumped models rely heavily on empirical correlations or values.

With the progress in understanding the physics behind the frost formation process, 1D semi-empirical models were developed. The frost thermal conductivity is still considered an averaged property for the frost layer, but temperature and local vapor density variation are considered. The common assumptions for 1D semi-empirical models are:

- The frost layer energy storage is neglected (K.-S. Lee et al., 1997; Qiao et al., 2017).
- One-dimensional heat and mass transport process (frost properties vary in the direction of frost growth) (K.-S. Lee et al., 1997; Qiao et al., 2017).

- The frost layer is characterized by average properties (thermal conductivity) (K.-S. Lee et al., 1997; Qiao et al., 2017).
- Frost thermal conductivity is only dependent upon the average frost density (K.-S. Lee et al., 1997; Qiao et al., 2017).
- Convection and radiation heat transfer within the frost layer is negligible (K.-S. Lee et al., 1997; Qiao et al., 2017).
- Simultaneous heat and mass transfer follows the Lewis analogy (K.-S. Lee et al., 1997; Qiao et al., 2017).
- Ideal gas law is applied for water vapor (K.-S. Lee et al., 1997; Qiao et al., 2017).
- The frost thickness is the same for the tube and fin in each segment, or the frost thickness is the same along the airflow direction (K.-S. Lee et al., 1997; Qiao et al., 2017).
- Fick's law for water vapor diffusion (K.-S. Lee et al., 1997; Qiao et al., 2017).

During the frost formation process, both frost layer density and frost layer thickness increase. The mass flow rate contribution to the frost density increase is related to the water vapor absorption rate within the frost layer. 1D semi-empirical models can be classified by the assumptions on the water vapor absorption rate. Some literature assumed that the local water vapor absorption rate in the frost layer is proportional to the local water vapor density (El Cheikh & Jacobi, 2014; Hermes, 2012; K.-S. Lee et al., 1997; Qiao et al., 2017). With correct boundary conditions on the frost surface and the wall, the local water vapor density and temperature profile can be calculated analytically (Hermes, 2012; K.-S. Lee et al., 1997, p. 19; Qiao et al., 2017) or numerically (El Cheikh & Jacobi, 2014). Another way to model water vapor absorption rate is assuming water vapor is saturated in the frost layer (Jones & Parker, 1975; Le Gall et al., 1997; Y. B. Lee & Ro, 2005). Clausius-Clapeyron is applied to convert the derivative of local water vapor density to the derivative of the local temperature. Then the temperature profile can be calculated using the energy balance equation. The frost densification mass flow rate is obtained using the temperature profile.

The lumped and 1D mathematical models focus only on the heat and mass transfer process in the frost layer. The air side is often considered uniform and serves as the boundary conditions. Computational fluid dynamics (CFD) models, on the other hand, mainly calculate the airflow distribution on the geometry, and its effect on the frost distribution on complex geometry. Therefore, CFD models are usually 2D or 3D so that they can calculate the distribution of the frost along the airflow direction (Kim et al., 2015). In contrast, lumped and 1D mathematical models assume that the frost thickness is uniform everywhere.

The CFD models can be classified into two categories, single-domain approach and two-domain approach. The two-domain approach is based on the Eulerian multiphase model. The primary phase is humid air, and the secondary phase is ice. Governing equations are solved in each phase. Interface matching conditions are used to balance the heat and the mass transfer between the two phases. Examples using the two-domain approach are K.-S. Lee et al. (2003) and Lenic et al. (2009). The single-domain approach only solves the governing equations in the humid air domain. The frost formation process is calculated as extra source terms and sink terms. The advantage of the single-domain approach is that it does not require the equations for the interface between the two phases, and it can also save computational time. Examples of the single-domain approach are Kim et al. (2015) and Wu et al. (2017). Though the CFD models can reveal more physics phenomena than the semi-empirical models, they are limited by the computational cost. Changing the geometry of the heat exchanger also requires time to regenerate the mesh. These drawbacks make it unsuitable for integrating with heat pump system models.

2.3 Additional Model Details

Due to the complexity of frost characteristics, it is necessary to apply empirical correlations in first-principle models. The most common empirical correlation used in the first-principle models is for frost thermal conductivity. The frost thermal conductivity is affected by the frost density, structure of the frost layer, internal diffusion of the water vapor caused by temperature distribution in a frost layer, and eddy generated by the roughness of the frost surface (Hayashi et al., 1977). However, for the sake of simplicity, the widely adopted frost thermal conductivity is correlated with the frost density. Yonko & Sepsy (1967) developed an empirical correlation for the frost thermal conductivity as a function of the frost density, as shown in Equation (1).

$$k_f = 0.02422 + 7.214 \cdot 10^{-4} \cdot \rho_f + 1.1797 \cdot 10^{-6} \cdot \rho_f^2 \quad (1)$$

Similarly, K. S. Lee et al. (1994) also correlated the frost thermal conductivity with the frost density.

$$k_f = 0.132 + 3.13 \times 10^{-4}\rho_f + 1.6 \times 10^{-7}\rho_f^2 \quad (2)$$

Another correlation for the frost thermal conductivity as a function of density is shown in Equation (3), developed by O'Neal & Tree (1984).

$$k_f = 1.202 \times 10^{-3}\rho_f^{0.963} \quad (3)$$

where k_f is the frost thermal conductivity in W/m-K, and ρ_f is the frost density in kg/m^3 for all these correlations. A comparison of these correlations is shown in Figure 2.

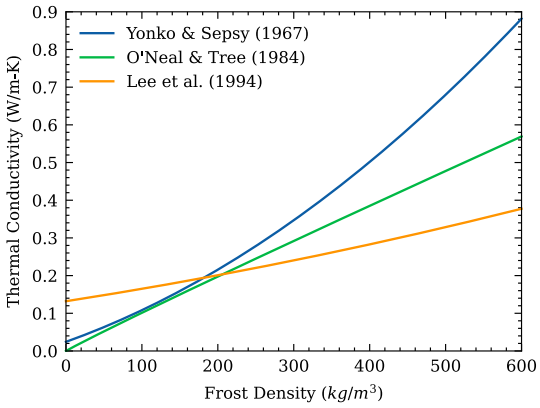

Figure 2: Comparison of thermal conductivity correlations

The empirical correlations for the frost density can simplify the modeling for frost formation even further. The most commonly used correlation for the frost density is a function of the frost surface temperature, as shown in Equation (4) (Hayashi et al., 1977).

$$\rho_f = 650 \cdot \exp\left(0.277 \cdot T_{fs}\right) \quad (4)$$

where ρ_f is the frost density in kg/m^3, and T_{fs} is the frost surface temperature in °C. Later, Hermes et al. (2009) improved the correlation to Equation (5). It was also used in Hermes (2012).

$$\rho_f = 207.3 \exp\left(0.266T_{fs} + 0.0615T_w\right) \quad (5)$$

where ρ_f is the frost density in kg/m^3, T_{fs} is the frost surface temperature in °C, and T_w is the wall temperature in °C. Then the correlation for the density was further improved to be a function of frost surface temperature and air stream dewpoint temperature (da Silva et al., 2011).

$$\rho_f = 494 \exp\left(0.11\, T_{fs} - 0.06T_{dew}\right) \quad (6)$$

where ρ_f is the frost density in kg/m^3, T_{fs} is the frost surface temperature in °C, and T_{dew} is the air stream dewpoint temperature in °C. In another journal article from the same author, the empirical correlation for density was changed to Equation (7) (Knabben et al., 2011).

$$\rho_f = 492.95 \exp\left(0.053\, T_w - 0.053T_{dew}\right) \quad (7)$$

where ρ_f is the frost density in kg/m^3, T_w is the wall temperature in °C, and T_{dew} is the air stream dewpoint temperature in °C. This reveals the shortcoming of using empirical correlations for frost density. If the experimental conditions change, the correlation also must change to get accurate predictions.

Frost thickness is often calculated using first-principle models. Only early studies correlate the frost thickness to the frost surface temperature, wall temperature, and time, as shown in Equation (8) (Cremers & Mehra, 1982). The frost surface temperature, wall temperature, and time are all measured from experiments. According to the authors' measurements, the frost surface temperature is constant as the frost grows. The frost surface temperature is close to the triple point in high humidity cases, and is lower than the triple point in low humidity cases.

$$\delta_f = 0.12\left[t\left(T_{fs} - T_w\right)\right]^{0.43} \tag{8}$$

where t is the time in minutes, T_{fs} is the frost surface temperature in K, T_w is the wall temperature in K, and δ_f is the frost thickness in mm.

The impact of frost formation on heat transfer rate of the heat exchanger is mainly due to the thermal resistance of the porous frost layer, which is calculated through the frost formation model. Because the frost layer does not change the heat exchanger geometry, the fin efficiency of the heat exchanger remains the same. However, the frost layer changes the flow resistance of each tube segment in the heat exchanger, causing airflow redistribution on the heat exchanger. The airflow redistribution calculation should be synchronized with frosting model by assuming that the airflow is at steady state for each time step of the frosting model. The air mass flow rate change can be calculated by setting the pressure drop for each tube segment the same as the pressure increase on the fan. It can be calculated using an iteration approach (Padhmanabhan et al., 2011) or an iteration-free approach (Qiao et al., 2017).

2.4 Discussion

In essence, the frost growth processes were investigated and divided into stages in previous studies. Since the first two stages are fast and difficult to model, early semi-empirical models ignored the first two stages and only picked the initial frost thickness and density for modeling Stage 3. Newer CFD models still treated the frost layer as a porous medium but calculated frost thickness, density, and thermal conductivity through all three stages. In addition, semi-empirical models used correlations for frost properties. While the early-stage models used more correlations, the most commonly used semi-empirical model nowadays only used the correlation for frost thermal conductivity as a function of density. Newer CFD models did not require the use of empirical correlations. CFD models can also account for the geometry difference in modeling frost formation on heat exchangers, but they are also limited by complexity in implementation and computation time. In general, the models match well with the experiments. They should be accurate enough if someone wants to use either semi-empirical or CFD models. However, the initial conditions play an important part in the results of semi-empirical models. The CFD models are limited by their complexity. Future research on frost formation modeling could focus on reducing the complexity of the CFD models or further improving the semi-empirical models using the results from the CFD models.

3. DEFROST MODELING

3.1 Defrost Process Overview

The defrost process aims to remove the frost after it forms on the outdoor heat exchanger surfaces. The most common defrost methods are electric heating defrosting (EHD), hot gas bypass defrosting (HGBD), and reverse cycle defrosting (RCD). There are many publications that compare the performance of different defrost techniques (Huang et al., 2009; Klingebiel et al., 2023; Ye et al., 2021). Many researchers reported that RCD is the most effective compared to the other options such as EHD or HGBD. For example, Huang et al. reported that RCD takes 65% less defrost time than HGBD (Huang et al., 2009). Klingebiel et al. showed that RCD had the highest defrost efficiency (56%−61%) compared to warm brine defrost with a supply temperature of 30°C (16%−45%) and EHD (44%−45%) (Klingebiel et al., 2023). Ye et al. showed RCD electric energy use was 82.5% less than that of HGBD (Ye et al., 2021). Different

defrosting methods presents different frost melting paradigms. For RCD and HGBD, the heat is provided by the hot refrigerant vapor in the tube, so the melting starts from the tube/fin. For EHD, the heat transfer direction might be different, depending on the installed location of the heater.

In this paper, we focus on the modeling of RCD and HGBD with heat supplied from the refrigerant side. The frost in direct contact with the tube and fins starts to melt first. Then, a thin water layer forms between the tube and the fin surface and the frost layer. The maximum thickness of the water layer is a result of gravity, heat exchanger orientation, geometry, and surface energy. After the thickness of the water layer reaches a maximum, some studies concluded that an air gap formed between the water layer and the frost layer (Dopazo et al., 2010; Qiao et al., 2018). Other studies (Qu et al., 2012; Song et al., 2014) concluded that an air gap did not exist. According to these models, the thickness of the frost layer decreases, but the frost layer is still in contact with the water layer. When the thickness of the frost layer is 5% of its initial value (Dopazo et al. 2010), it falls off from the heat exchanger. When the thickness of the frost reaches zero, the retained water layer starts vaporizing, until the water layer thickness reaches zero.

A physics-based defrosting model is important to predict the heat pump energy use accurately during defrost cycles. Physics-based models can provide accurate outdoor coil temperature for heat pump performance calculations, while empirical models rely on outdoor air temperature. In addition, physics-based models can provide accurate duration for each stage in the defrosting process. However, empirical models use the defrosting time duration from the defrost control strategy. Therefore, physics-based models can predict more accurate energy use for each stage, even for the dry heating stage, which can be used for optimizing defrost control strategies.

3.2 Model Formulation

The pioneering defrost model was put forward by Krabow et al. (1993), in which the defrost process was divided into preheating, melting, vaporizing, and dry heating. This multi-stage paradigm formed the foundation for the subsequent studies that further developed the defrost models. Table 1 summarizes the first-principle defrost models. As shown in the table, the models developed later became more and more comprehensive, adding considerations such as heat exchanger (HX) circuitry, gravity effect, and heat pump transients between frost and defrost. Embedding a defrost model with a distributed-parameter, multi-circuitry HX model allows the description of uneven defrosting (e.g., some surface is in the dry heating stage while other surfaces are still in the melting stage). Some models try to account for the melted frost flowing downward and draining away. Heat pump transients refer to the integration of an HX model into the system model that captures the refrigerant transients during the initiation and termination of the defrost period.

Table 1 Summary of first-principle based defrost model

Reference	Multiple defrost stages	Multi-circuitry HX model	Melted frost flowing due to gravity	Heat pump transients between frost and defrost
(Dopazo et al., 2010; Krakow et al., 1993)	√	×	×	×
(Qu et al., 2012; Song et al., 2014)	√	√	√	×
(Ma et al., 2023; Qiao et al., 2018)	√	√	×	√
(Han et al., 2022)	√	×	×	√
(Xiong et al., 2024)	√	×	√	√

Dopazo et al. (2010) divided the defrosting process into five stages. The first stage, preheating, ended when the temperature of the frost on the tubes reached the melting point. The second stage was the tube frost melting stage. During the second stage, a water film formed between the tube surface and the frost. This stage ended when the fin surface reached the melting point. Therefore, the third stage was the fin frost melting stage. This stage ended when an

air gap formed between the water layer and the frost. During the fourth stage, the air presence stage, the air gap grew, and the frost layer thickness decreased, until it was 5% of its initial value. The fifth stage was the water film evaporation stage. Energy balance for the tubes and fins were considered separately. Qiao et al. (2018) adopted a similar approach as Dopazo et al. (2010), but combined the tubes and the fins into an integral system. Therefore, Stage 2 and Stage 3 from Dopazo et al. (2010) were combined into the same stage. The air presence stage from Qiao et al. (2018) did not end with 5% of the frost falling off the heat exchanger, but all the frost was melted in this stage. An additional stage, the dry heating stage, was added at the end of the defrosting process.

Qu et al. (2012) and Song et al. (2014) adopted a different approach. Qu et al. (2012) divided the defrosting process into three stages. The first stage was frost melting without water flow. During this stage, the water layer thickness increased because of the heat transfer from the refrigerant. The water layer temperature increased as well. This stage continued until the water layer reached its maximum thickness. The second stage was frost melting with water flow. During this stage, the frost layer thickness kept decreasing, but was still in contact with the water layer. The extra water flew from the upper control volume to the lower control volume. This stage ended when the frost layer disappeared. The third stage was the water layer vaporization stage. During this stage, all the outdoor coils were free of frost. The heat transfer from the refrigerant contributed to the water layer temperature, evaporation, and convection on the surface covered by water or surface without water. Song et al. (2014) modified the stages by adding a preheating stage to the previous study. The stage, frost melting with water flow, was modified by taking into account the convection on the surface covered by water and frost, instead of only frost-air convection in Qu et al. (2012).

Very limited studies were found to draw on CFD to visualize or investigate the defrost process on an HX, except for a master thesis published in 2010 (Ha, 2010). The author developed a 3D model in CFD to simulate the frost melting on a section of a tube-fin HX and used the model to investigate the effect of hot gas temperature. However, abundant papers were found to use CFD models to predict the defrost process on an automotive windshield. The absence of tube-fin HX defrost CFD models could be due to the complexity of the defrost process, that, unlike the frosting formation process, does not originate from the heat and mass transfer process itself (the defrost problem on a flat surface can be formulated as a standard thermal resistance network problem). The biggest complexity comes from the gravity effect that removes the melted frost from the HX surface and from the multi-circuitry HX geometry, potentially making CFD not the best simulation tool.

3.3 Discussion

RCD and HGBD defrosting processes were divided into stages by previous studies. First-principle models were developed based on the stage division. After the thickness of the water layer reaches a maximum, some studies concluded that an air gap formed between the water layer and the frost layer, while other studies concluded that the air gap did not exist. However, until now, there has been no experimental evidence to validate either one. Previous studies also disagreed on the amount of frost or water falling down from the heat exchanger at the end of the melting process. No experimental data can validate that amount.

4. INTEGRATION WITH HEAT PUMP AND BUILDING MODELS

4.1 Integration with Heat Pumps

The models that we reviewed above are useful tools for heat exchanger design. On the other hand, many researchers are interested in the effect of defrosting on heat pump operation and occupants' thermal comfort (power consumption, capacity degradation, indoor air temperature, etc.). Therefore, integrating the frost and defrost models with heat pump/building models is necessary. There are, in general, two groups of methods to integrate the defrosting aspect into a heat pump model: physics-based approaches or empirical approaches. Previous studies have integrated first-principle frosting and defrosting models with detailed heat pump equipment models. Qiao (2014) integrated first-principle frosting and defrosting models into a discretized heat exchanger model. The discretized heat exchanger model was combined with other component models to form a platform in Modelica that can perform transient simulations for vapor compression systems. The transient models could predict the performance of a flash tank vapor injection heat pump system under frosting conditions and during reverse-cycle defrosting cycles. Ma et al. (2023) integrated a similar first-principle frosting and defrosting model with a segment-by-segment finite-volume heat exchanger model. The five-stage defrosting process was modified using the Takagi-Sugeno fuzzy modeling method

to avoid numerical discontinuities and improve efficiency and robustness. Ma et al. (2023) then combined the heat exchanger model with other component models and developed a transient heat pump model in Modelica. The authors were able to use the transient heat pump model to predict the performance of a variable-speed R410A heat pump under frosting and defrosting conditions.

Some research directly studied the impact of frosting and defrosting on heat pumps by empirical approaches. Zhu et al. (2015) divided the outdoor dry bulb temperature and relative humidity by zones, and correlated these outdoor conditions to the defrost time interval. Similarly, Shao et al. (2021) directly related the heat pump COP deterioration factor to the zones of the outdoor conditions, and analyzed the thermodynamic performance and economic potential of an air-source heat pump with direct-condensation radiant panel.

4.2 Influence on Buildings

These empirical correlations enable high-level impact analysis of heat pump operation without the detailed knowledge of the frost buildup process. Due to low model fidelity and computational cost, this type of analysis can be easily incorporated with building energy modeling (e.g., E+ or TRNSYS) and scaled up to a large geographical or temporal scale. EnergyPlus used an empirical approach to determine the defrost time fraction as a function of outdoor humidity ratio and used defrost energy input ratio with respect to outdoor dry bulb temperature and indoor dewpoint temperature to determine the heat pump performance during defrost cycles (DOE, 2022). The defrost energy use results were averaged during each EnergyPlus time step. This method could provide a rough estimate of the annual defrosting energy use, but was not able to provide information about the peak demand. This method also could not determine the frost thickness, defrost cycle initiation frequency, and the amount of dry heating time during defrost cycles, which can be solved by first-principle models. Dongellini et al. (2019) determined the defrost power, defrost time interval, defrost cycle duration, heat pump COP, and heating capacity degradation under frosting conditions as a function of outdoor dry bulb temperature and relative humidity. The performance of the air-to-water heat pump was then assessed in TRNSYS for different climates. Gollamudi et al. (2022) applied the heat pump COP deterioration factor due to frosting from Shao et al. (2021) and compared the greenhouse gas emissions of a heat pump to a natural gas furnace. Due to defrost cycles and the current greenhouse gas intensity of the electric grid, ASHP retrofitting is not favored in Saskatoon, Canada.

4.3 Discussion

Previous studies investigated the influence of frosting and defrosting on heat pumps using transient simulation, the results were validated with experiments. The modeling of the influence of frosting and defrosting on buildings still relies on the degradation factors for simplicity. There is no validation for the degradation approach used by EnergyPlus and other previous studies.

5. CONCLUSIONS

This article reviewed numerical models for frost formation and defrosting related to HVAC&R application. We began with background information about frosting and defrosting on heat exchangers and their impact on heat pump operation. For frost formation models, we reviewed the first-principle models on simple geometries, including the common assumptions and various methods to determine the frost densification rate and frost growth rate. In addition, empirical correlations for frost characteristics were discussed and compared. For defrosting models, the multi-stage defrost process was presented. There are, in general, two modeling approaches, with the key differentiator being whether the model assumes the presence of air gap and water flow. The formulations from different studies were compared. Lastly, physics-based and empirical approaches were discussed to integrate defrosting into higher level heat pump/building models.

Potential future research on this topic includes further evaluation of the air gap assumption in the defrost models, and a representation method to characterize the frost falling from the heat exchanger. Moreover, the previous literature presents a clear disconnection between the high-fidelity equipment-level models and the empirical models used in high-level impact analysis. There is a need to develop a generalized approach to enable large temporal/geographical scale analysis with the detailed equipment models.

NOMENCLATURE

ρ	density	(kg/m^3)
k	thermal conductivity	(W/m-K)
T	temperature	(°C)
Subscript		
f	frost	
fs	frost surface	
w	wall	
dew	dewpoint	
Acronym		
ASHP	air-source heat pump	
CFD	computational fluid dynamics	
COP	coefficient of performance	
DBG	densification and bulk growth	
DWC	dropwise condensation	
EHD	electric heating defrost	
HGBD	hot gas bypass defrost	
HX	heat exchanger	
RCD	reverse cycle defrost	
STG	solidification and tip-growth	

REFERENCES

Badri, D., Toublanc, C., Rouaud, O., & Havet, M. (2021). Review on frosting, defrosting and frost management techniques in industrial food freezers. *Renewable and Sustainable Energy Reviews*, *151*, 111545. https://doi.org/10.1016/j.rser.2021.111545

Cremers, C. J., & Mehra, V. K. (1982). Frost Formation on Vertical Cylinders in Free Convection. *Journal of Heat Transfer*, *104*(1), 3–7. https://doi.org/10.1115/1.3245065

da Silva, D. L., Hermes, C. J. L., & Melo, C. (2011). First-principles modeling of frost accumulation on fan-supplied tube-fin evaporators. *Applied Thermal Engineering*, *31*(14), 2616–2621. https://doi.org/10.1016/j.applthermaleng.2011.04.029

DOE, U. S. A. (2022). *EnergyPlus Engineering Reference*.

Dongellini, M., Piazzi, A., Biagi, F. D., & Morini, G. L. (2019). The modelling of reverse defrosting cycles of air-to-water heat pumps with TRNSYS. *E3S Web of Conferences*, *111*, 01063. https://doi.org/10.1051/e3sconf/201911101063

Dopazo, J. A., Fernandez-Seara, J., Uhía, F. J., & Diz, R. (2010). Modelling and experimental validation of the hot-gas defrost process of an air-cooled evaporator. *International Journal of Refrigeration*, *33*(4), 829–839. https://doi.org/10.1016/j.ijrefrig.2009.12.027

El Cheikh, A., & Jacobi, A. (2014). A mathematical model for frost growth and densification on flat surfaces. *International Journal of Heat and Mass Transfer*, *77*, 604–611. https://doi.org/10.1016/j.ijheatmasstransfer.2014.05.054

Fossa, M., & Tanda, G. (2002). Study of free convection frost formation on a vertical plate. *Experimental Thermal and Fluid Science*, *26*(6), 661–668. https://doi.org/10.1016/S0894-1777(02)00173-5

Gollamudi, S., Krishnana, E., Ramin, H., Annadurai, G., & Simonson, C. (2022, November 25). MODELLING AIR-SOURCE HEAT PUMPS IN COLD CLIMATIC CONDITIONS CONSIDERING THE EFFECTS OF FROSTING. *3rd IBPSA Scotland Conference Urban Energy in a Net Zero World*. uSIM2022, Glasgow, Scotland.

Ha, O. T. (2010). *Modeling and Numerical Investigation of Hot Gas Defrost on a Finned Tube Evaporator Using Computational Fluid Dynamics: A Thesis* [PhD Thesis]. California Polytechnic State University.

Han, B., Xiong, T., Xu, S., Liu, G., & Yan, G. (2022). Parametric study of a room air conditioner during defrosting cycle based on a modified defrosting model. *Energy*, *238*, 121658. https://doi.org/10.1016/j.energy.2021.121658

Hayashi, Y., Aoki, A., Adachi, S., & Hori, K. (1977). Study of Frost Properties Correlating With Frost Formation Types. *Journal of Heat Transfer*, *99*(2), 239–245. https://doi.org/10.1115/1.3450675

Hermes, C. J. L. (2012). An analytical solution to the problem of frost growth and densification on flat surfaces. *International Journal of Heat and Mass Transfer*, *55*(23), 7346–7351. https://doi.org/10.1016/j.ijheatmasstransfer.2012.06.070

Hermes, C. J. L., Piucco, R. O., Barbosa, J. R., & Melo, C. (2009). A study of frost growth and densification on flat surfaces. *Experimental Thermal and Fluid Science*, *33*(2), 371–379. https://doi.org/10.1016/j.expthermflusci.2008.10.006

Huang, D., Li, Q., & Yuan, X. (2009). Comparison between hot-gas bypass defrosting and reverse-cycle defrosting methods on an air-to-water heat pump. *Applied Energy*, *86*(9), 1697–1703. https://doi.org/10.1016/j.apenergy.2008.11.023

Iragorry, J., Tao, Y.-X., & Jia, S. (2004). Review Article: A Critical Review of Properties and Models for Frost Formation Analysis. *HVAC&R Research*, *10*(4), 393–420. https://doi.org/10.1080/10789669.2004.10391111

Jones, B. W., & Parker, J. D. (1975). Frost Formation With Varying Environmental Parameters. *Journal of Heat Transfer*, *97*(2), 255–259. https://doi.org/10.1115/1.3450350

Kim, D., Kim, C., & Lee, K.-S. (2015). Frosting model for predicting macroscopic and local frost behaviors on a cold plate. *International Journal of Heat and Mass Transfer*, *82*, 135–142. https://doi.org/10.1016/j.ijheatmasstransfer.2014.11.048

Klingebiel, J., Hassan, M., Venzik, V., Vering, C., & Müller, D. (2023). Efficiency comparison between defrosting methods: A laboratory study on reverse-cycle defrosting, electric heating defrosting, and warm brine defrosting. *Applied Thermal Engineering*, *233*, 121072. https://doi.org/10.1016/j.applthermaleng.2023.121072

Knabben, F. T., Hermes, C. J. L., & Melo, C. (2011). In-situ study of frosting and defrosting processes in tube-fin evaporators of household refrigerating appliances. *International Journal of Refrigeration*, *34*(8), 2031–2041. https://doi.org/10.1016/j.ijrefrig.2011.07.006

Krakow, K., Lin, S., & Yan, L. (1993). An Idealized Model of Reversed-Cycle Hot Gas Defrosting–Part 2: Experimental Analysis and Validation. *ASHRAE Transactions-American Society of Heating Refrigerating Airconditioning Engin*, *99*(2), 329–338.

Le Gall, R., Grillot, J. M., & Jallut, C. (1997). Modelling of frost growth and densification. *International Journal of Heat and Mass Transfer*, *40*(13), 3177–3187. https://doi.org/10.1016/S0017-9310(96)00359-6

Lee, K. S., Lee, T. H., & Kim, W. S. (1994). Heat and Mass Transfer of Parallel Plate Heat Exchanger under Frosting Condition. *Korean Journal of Air-Conditioning and Refrigeration Engineering*, *6*(2), 155–165.

Lee, K.-S., Jhee, S., & Yang, D.-K. (2003). Prediction of the frost formation on a cold flat surface. *International Journal of Heat and Mass Transfer*, *46*(20), 3789–3796. https://doi.org/10.1016/S0017-9310(03)00195-9

Lee, K.-S., Kim, W.-S., & Lee, T.-H. (1997). A one-dimensional model for frost formation on a cold flat surface. *International Journal of Heat and Mass Transfer*, *40*(18), 4359–4365. https://doi.org/10.1016/S0017-9310(97)00074-4

Lee, Y. B., & Ro, S. T. (2005). Analysis of the frost growth on a flat plate by simple models of saturation and supersaturation. *Experimental Thermal and Fluid Science*, *29*(6), 685–696. https://doi.org/10.1016/j.expthermflusci.2004.11.001

Lenic, K., Trp, A., & Frankovic, B. (2009). Transient two-dimensional model of frost formation on a fin-and-tube heat exchanger. *International Journal of Heat and Mass Transfer*, *52*(1), 22–32. https://doi.org/10.1016/j.ijheatmasstransfer.2008.06.005

Léoni, A., Mondot, M., Durier, F., Revellin, R., & Haberschill, P. (2016). State-of-the-art review of frost deposition on flat surfaces. *International Journal of Refrigeration*, *68*, 198–217. https://doi.org/10.1016/j.ijrefrig.2016.04.004

Li, S.-M., & Wang, C.-C. (2021). Predictive models on the frost formation for plain surface—A review and comparative study. *International Communications in Heat and Mass Transfer*, *129*, 105670. https://doi.org/10.1016/j.icheatmasstransfer.2021.105670

Ma, J., Kim, D., Braun, J. E., & Horton, W. T. (2023). Development and validation of a dynamic modeling framework for air-source heat pumps under cycling of frosting and reverse-cycle defrosting. *Energy*, *272*, 127030. https://doi.org/10.1016/j.energy.2023.127030

O'Neal, D., & Tree, D. R. (1984). Measurement of frost growth and density in a parallel plate geometry. *ASHRAE Transactions*, *90*, 278–290.

Padhmanabhan, S. K., Fisher, D. E., Cremaschi, L., & Moallem, E. (2011). Modeling non-uniform frost growth on a fin-and-tube heat exchanger. *International Journal of Refrigeration*, *34*(8), 2018–2030. https://doi.org/10.1016/j.ijrefrig.2011.06.005

Qiao, H. (2014). *Transient modeling of two-stage and variable refrigerant flow vapor compression systems with frosting and defrosting* [PhD Thesis, University of Maryland, College Park]. https://search.proquest.com/openview/5c459e4e95523fa9e0ab1472d752661b/1?pq-origsite=gscholar&cbl=18750

Qiao, H., Aute, V., & Radermacher, R. (2017). Dynamic modeling and characteristic analysis of a two-stage vapor injection heat pump system under frosting conditions. *International Journal of Refrigeration*, *84*, 181–197. https://doi.org/10.1016/j.ijrefrig.2017.08.020

Qiao, H., Aute, V., & Radermacher, R. (2018). Modeling of transient characteristics of an air source heat pump with vapor injection during reverse-cycle defrosting. *International Journal of Refrigeration*, *88*, 24–34. https://doi.org/10.1016/j.ijrefrig.2017.12.017

Qu, M., Pan, D., Xia, L., Deng, S., & Jiang, Y. (2012). A study of the reverse cycle defrosting performance on a multi-circuit outdoor coil unit in an air source heat pump – Part II: Modeling analysis. *Applied Energy*, *91*(1), 274–280. https://doi.org/10.1016/j.apenergy.2011.08.036

Shao, S., Zhang, H., Fan, X., You, S., Wang, Y., & Wei, S. (2021). Thermodynamic and economic analysis of the air source heat pump system with direct-condensation radiant heating panel. *Energy*, *225*, 120195. https://doi.org/10.1016/j.energy.2021.120195

Song, M., & Dang, C. (2018). Review on the measurement and calculation of frost characteristics. *International Journal of Heat and Mass Transfer*, *124*, 586–614. https://doi.org/10.1016/j.ijheatmasstransfer.2018.03.094

Song, M., Deng, S., & Xia, L. (2014). A semi-empirical modeling study on the defrosting performance for an air source heat pump unit with local drainage of melted frost from its three-circuit outdoor coil. *Applied Energy*, *136*, 537–547. https://doi.org/10.1016/j.apenergy.2014.09.012

Tan, H., Zhang, X., Zhang, L., Tao, T., & Xu, G. (2019). Ultrasonic influence mechanism of a cold surface frosting process and an optimised defrosting technique. *Applied Thermal Engineering*, *153*, 113–127. https://doi.org/10.1016/j.applthermaleng.2019.01.094

Tao, Y.-X., Besant, R. W., & Rezkallah, K. S. (1993). A mathematical model for predicting the densification and growth of frost on a flat plate. *International Journal of Heat and Mass Transfer*, *36*(2), 353–363. https://doi.org/10.1016/0017-9310(93)80011-I

Thakkar, A., Ma, J., Braun, J. E., Travis Horton, W., & Arrieta, A. F. (2023). Energy-efficient defrosting of heat exchanger fins with embedded negative stiffness structures. *Applied Thermal Engineering*, *222*, 119850. https://doi.org/10.1016/j.applthermaleng.2022.119850

Vocale, P., Morini, G. L., & Spiga, M. (2014). Influence of Outdoor Air Conditions on the Air Source Heat Pumps Performance. *Energy Procedia*, *45*, 653–662. https://doi.org/10.1016/j.egypro.2014.01.070

White, J. E., & Cremers, C. J. (1981). Prediction of Growth Parameters of Frost Deposits in Forced Convection. *Journal of Heat Transfer*, *103*(1), 3–6. https://doi.org/10.1115/1.3244426

Wu, X., Ma, Q., & Chu, F. (2017). Numerical Simulation of Frosting on Fin-and-Tube Heat Exchanger Surfaces. *Journal of Thermal Science and Engineering Applications*, *9*(031007). https://doi.org/10.1115/1.4035925

Xiong, T., Chen, Q., Xu, S., Liu, G., Gao, Q., & Yan, G. (2024). A new defrosting model for microchannel heat exchanger heat pump system considering the effects of drainage and water retention. *Energy*, *289*, 129968. https://doi.org/10.1016/j.energy.2023.129968

Ye, Z., Wang, Y., Yin, X., Song, Y., & Cao, F. (2021). Comparison between reverse cycle and hot gas bypass defrosting methods in a transcritical CO2 heat pump water heater. *Applied Thermal Engineering*, *196*, 117356. https://doi.org/10.1016/j.applthermaleng.2021.117356

Yonko, J. D., & Sepsy, C. F. (1967). An investigation of the thermal conductivity of frost while forming on a flat horizontal plate. *ASHRAE Transactions*, *73*(2), 1–1.

Zhu, J. H., Sun, Y. Y., Wang, W., Deng, S. M., Ge, Y. J., & Li, L. T. (2015). Developing a new frosting map to guide defrosting control for air-source heat pump units. *Applied Thermal Engineering*, *90*, 782–791. https://doi.org/10.1016/j.applthermaleng.2015.06.076

ACKNOWLEDGMENT

This work was authored by the National Renewable Energy Laboratory, operated by Alliance for Sustainable Energy, LLC, for the U.S. Department of Energy (DOE) under Contract No. DE-AC36-08GO28308. Funding was provided by the U.S. Department of Energy Office of Energy Efficiency and Renewable Energy Building Technologies Office. The views expressed in the article do not necessarily represent the views of the DOE or the U.S. Government. The